Hindawi
Shock and Vibration
Volume 2017, Article ID 7874543, 12 pages
https://doi.org/10.1155/2017/7874543

Research Article

Projectile Penetration into Sandy Soil Confined by a Honeycomb-Like Structure

Weiming Luo, Shaoqing Shi, Zipeng Chen, Jianhu Sun, and Wenkang Wang

Department of Civil Engineering, Logistical Engineering University, Chongqing 401311, China

Correspondence should be addressed to Weiming Luo; lwmofficial@163.com

Received 31 March 2017; Revised 6 August 2017; Accepted 24 August 2017; Published 3 October 2017

Academic Editor: Enrico Zappino

HPS (Honeycomb-like Protective Structure) is a newly proposed protective structure filled with sandy soil. In order to investigate the penetration resistance of the structure, numerical simulations based on SPH method had been carried out by using LS-DYNA, which are corresponding to the experiments. The calibrated model leads to reasonable predictions of the dynamic responses and damage modes of the HPS. More situations were carried out taking factors influencing the penetration into consideration, including point of impact, angle of impact, and projectile caliber. Penetration mode was established by analyzing the energy dissipation and investigating the mechanism from the phenomenological viewpoint. Simulation results show that the resisting forces and the torque that act on the long rod projectile would be greater than those acting on the short one when instability occurred. Besides, approximate 45° angle of impact was formed in the case of off-axis, which has a certain influence on the ballistic stability, resulting in more kinetic energy of projectile dissipating in HPS and less depth of penetration. The kinetic energy of projectile dissipated in sandy soil largely and the strip slightly, and the former was greater than the sum of the latter.

1. Introduction

With the increase of local war and terrorist attack in recent years, protective structure is widely used in military, antiterrorism, and peacekeeping operations. In particular, in the time before and during the establishment of new camps, it is important to build protective structure within a shortest possible period of time. Long-distance transportation of the protective elements is required in most cases, and the weight of the system is thus a critical parameter. Therefore, the protective structure filled with materials that can be obtained from local sources is developed nowadays. A gabion cage made of a hexagonal wire mesh was investigated under uniaxial compression to study its mechanical behavior [1], which was filled with sand and scrapped tires. Børvik et al. [2, 3] showed experimentally that AA6005-T6 aluminum panels filled with granular materials could be used with success to mitigate the possibly lethal effects of explosions and impacts by projectiles or debris. HESCO is a relatively common structure, which is foldable welded-wire mesh baskets with lined geotextile. When filled with soil, it forms protective walls and structures [4].

HPS (Honeycomb-like Protective Structure) is a newly proposed protective structure by the authors' team, which can be filled with sandy soil or other granular materials. It has good foldability which is convenient for transport and setting up. As an important factor of design and optimization, penetration resistance of the protective structure must be taken into consideration. In order to verify the penetration resistance of the structure, the ballistic experiment was carried out by the team. In total, 4 kinds of projectiles were used in the experiment, including MCPB (middle caliber pistol bullet), MCRB (middle caliber rifle bullet), SCPB (small caliber pistol bullet), and SCRB (small caliber rifle bullet). The experiment setup was shown in Figure 1. Figure 2 shows the projectile intercepted in the structure after experiment. The DOP (depth of penetration) was measured by instruments. The damage mode and failure phenomenon were observed after the experiment as well. The experiment results showed that the structure has a certain resistance when it was penetrated by small-arms projectile. However, it is still hard to analyze the process of penetration accurately during the whole experiment. Thus, it is necessary to study it further using other methods.

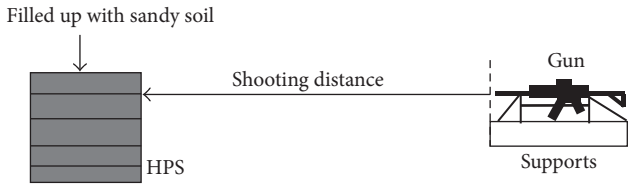

Figure 1: Experiment setup.

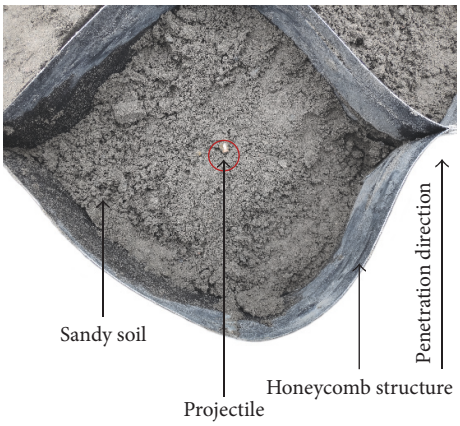

Figure 2: Projectiles intercepted in HPS.

Projectile penetrating into sand or sand-like soil is a localized phenomenon that the kinetic energy of projectile is dissipated into deformation and failure of target [5, 6]. To investigate the issue, empirical (semiempirical, phenomenological) models and analytical models were used [7]. Numerical simulations were also utilized due to their convenience, accuracy, and affordability. FEM (Finite Element Method) is the most common means of simulation. However, the main challenge of the FEM for high velocity penetration and perforation is the severe element distortion. A discrete particle method was used in combination with finite element analysis to describe the interaction between structures and granular media during ballistic impact [8]. By applying the method to model granular materials, issues like mesh distortion and element deletion were avoided. The results from the numerical simulations described the trends from the experiments, which was the perforation of empty and sand-filled aluminum alloy panels subjected to impacts by small-arms bullets. Similarly, a discrete particle-based approach was used to model the behavior of sand during bullet impact [9]. The method works with discrete particles that transfer forces between each other through contact and elastic collisions, allowing for a simple and robust treatment of the interaction between the sand particles and the bullet. An important observation from that study was that the penetration depth is strongly influenced by deviation of the bullet from its original trajectory. The three-dimensional FEM-DEM (Discrete Element Method) was also applied to the simulation of tire-sand interactions, where the tire was discretized into hexahedron finite elements and sand was modeled using the discrete element method [10]. The feasibility and effectiveness of the method were proven by comparing the simulation results with the experimental

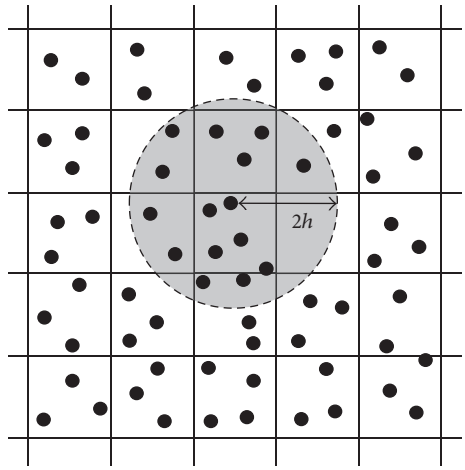

Figure 3: Interaction between SPH particles (Swaddiwudhipong et al. [11]).

results. Coupled FEM-SPH (Smooth Particle Hydrodynamics) method was also used to simulate penetration problem [11] and blast response issue [12]. In blast simulation, the SPH particles were used to model the explosive and the soil that experience large deformations, while the finite elements were used to model the rest of the soil and the tunnel. The modeling techniques were validated with the results from experiments involving the above and below ground explosions.

Due to the capability of handling large deformation without severe element distortion, SPH method was adopted to simulate that projectile penetrating into sandy soil which was confined by HPS. The key factors influencing the penetration including point of impact (POI), angle of impact (AOI), and projectile caliber were taken into consideration. Preprocessing function of ANSYS, LS-DYNA, and postprocessing function of LS-PrePost were applied to conduct the simulation.

2. Numerical Simulation Model

2.1. SPH Method. SPH is a computational technique for numerical simulation actually. Moreover, it is a Lagrangian formulation based method where the coordinates move with the object [11]. The computational domain is discretized into a finite number of particles. Every particle represents a certain volume and mass of the material, which carries field variables such as velocity, acceleration, density, and pressure/stress. The material properties at any point x in the domain are calculated according to an interpolation process over its neighboring particles. The SPH particles' self-interaction and interaction with FE are shown in Figures 3 and 4. The standard expression about the interaction is given below:

$$\prod^{h} f(x) = \int f(y) W(x - y, h)\, dy, \tag{1}$$

where W is the smoothing kernel function and y is location of the mass point. Smooth length h is a unit measure of the

Table 1: Material parameters in LS-DYNA.

Material	Mass density ρ (kg/m^3)	Poisson's ratio ν	E (GPa)
Projectiles	7850	0.35	210
Strip of HPS	970	0.45	1.03
Sandy soil	1726	0.35	31.8

subdomain of influence of function. The kernel function W can also be defined as

$$W(x,h) = \frac{1}{h(x)^d}\theta(x), \tag{2}$$

where d is the number of space dimensions. The most common kernel is B-spline which is defined as

$$\theta(u) = C \times \begin{cases} 1 - \dfrac{3u^2}{2} + \dfrac{3u^3}{4} & |u| \le 1 \\ \dfrac{(2-u)^3}{4} & 1 \le |u| \le 2 \\ 0 & |u| \ge 2, \end{cases} \tag{3}$$

where C is a constant of normalization determined by d. The kernel function must meet the basic conditions as follows.

Normalization is as follows:

$$\int_\Omega W(x-y,h)\,dy = 1. \tag{4}$$

Symmetry is as follows:

$$\int_\Omega (x-y)\,W(x-y,h)\,dy = 0. \tag{5}$$

Kernel function will tend to the delta function:

$$\lim_{h\to 0} W(x-y,h) = \delta(x-y). \tag{6}$$

If $f(x)$ is substituted by $\nabla \cdot f(x)$, the approximation of space derivative can be obtained:

$$\nabla \cdot f(y) = \int_\Omega \left[\nabla \cdot f(y)\,W(x-y,h)\right] dy, \tag{7}$$

where ∇ is the Hamilton operator. According to the definition of the divergence and Gauss theorem, the following expression can be obtained:

$$\nabla \cdot f(y) = -\int_\Omega f(y) \cdot \nabla W(x-y,h)\,dy. \tag{8}$$

2.2. Modeling. Projectile and HPS were created as FE (finite element) model by using ANSYS program. SOLID164 and SHELL163 elements were used to simulate the projectiles and HPS, respectively [13, 14]. The striking velocities (when projectile getting contact with the target) were set as the initial velocities of projectiles in simulation, which is shown in Table 2. SPH particles were generated by using LS-PrePost program [15, 16]. For the purpose of saving computing time

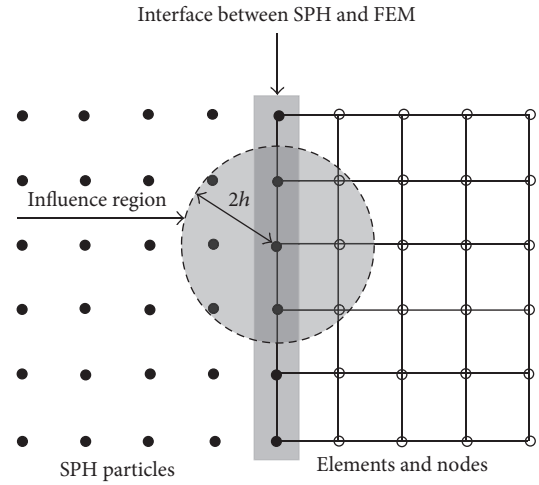

Figure 4: Interaction between SPH particles and FE (Swaddiwudhipong et al. [11]).

and storage space, all models were simplified as 1/2 symmetry models by defining the symmetrical boundary condition, as shown in Figure 5. The symmetry plane and GHOST particles were created. The soil-and-foam model was selected to simulate the sandy soil. The rigid body model was used to simulate the projectiles. The plasticity polymer model was selected to simulate the strip of the HPS. The parameters were obtained from literatures [17–20] and mechanical experiment, as listed in Table 1. The soil-and-foam model works in some ways like a fluid, which should be used only in situations where soils or foams are confined within a structure or where geometric boundaries are present. Volumetric strain is given by the natural log of the relative volume. Relative volume is a ratio of the current volume to the initial volume at the start of the calculation. If the pressure drops below the cutoff value specified, it is reset to that value. The deviatoric perfectly plastic yield function ϕ, which is described in terms of the second invariant, is as follows:

$$\begin{aligned} J_2 &= \frac{1}{2} \times S_{ij}S_{ij} \\ \phi &= J_2 - \left[a_0 + a_1 p + a_2 p^2\right], \end{aligned} \tag{9}$$

where p is pressure and a_0, a_1, and a_2 are constants. On the yield surface, $J_2 = 1/3 \times \sigma_y^2$, where σ_y is the uniaxial yield stress; that is,

$$\sigma_y = \left[3\left(a_0 + a_1 p + a_2 p^2\right)\right]^{1/2}. \tag{10}$$

There is no strain hardening on this surface. To eliminate the pressure dependence of the yield strength, set

$$\begin{aligned} a_1 &= a_2 = 0, \\ a_0 &= \frac{1}{3} \times \sigma_y^2. \end{aligned} \tag{11}$$

This method is useful when a Von Mises type elastic-plastic model is desired for use with the tabulated volumetric data.

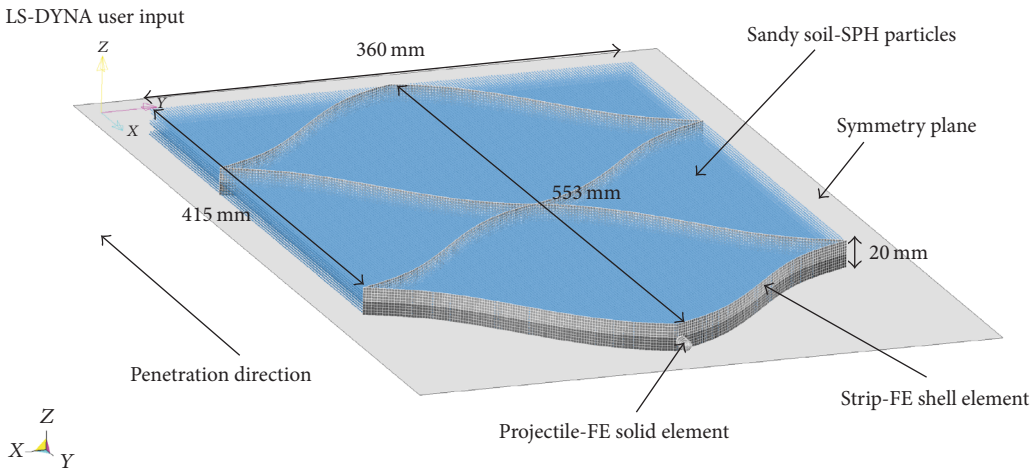

Figure 5: Sketch of simulation model.

Table 2: Properties of projectiles and the DOP data obtained from experiment and numerical simulations.

Projectile type	Caliber (mm)	Mass (g)	Muzzle velocity (m/s)	Striking velocity (m/s)	Striking energy (J)	DOP in test (mm)	DOP in simulation (mm)			
							Middle-axis	Error	Off-axis	Error
MCPB	7.62	5.5	420	358	352.5	239.6	252	5.18%	248	3.51%
MCRB	7.62	7.9	720	615	1494.0	253.4	273	7.73%	269	6.16%
SCPB	5.8	3.0	490	379	215.5	170.2	182	6.93%	179	5.17%
SCRB	5.8	4.2	930	846	1503.0	195.3	208	6.50%	202	3.43%

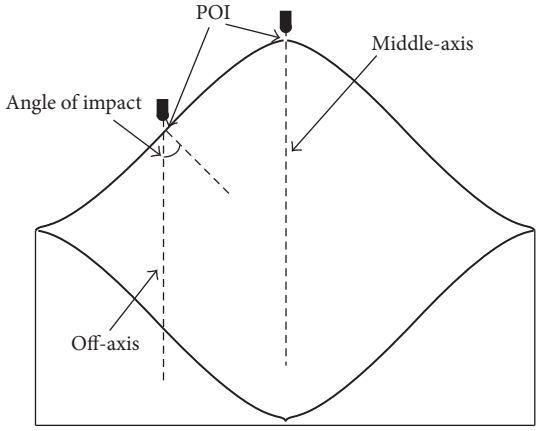

Figure 6: Two points of impact.

2.3. Model Calibration and Discussion. For comparison, numerical simulations which were corresponding to the experiments were carried out; the DOP data, negative acceleration, and process of energy transfer were obtained. Calibers, mass, velocities (including muzzle velocity and striking velocity), and energy of projectiles and mean values of DOP data obtained from experiment and numerical simulations are listed in Table 2. A total of 24 valid tests were performed. For each projectile, there were 6 times shooting, of which 3 times were aimed at middle-axis and 3 times were aimed at off-axis. However, due to the firing accuracy in experiment, about 95% of the POI (point of impact) distributed on two sides of the honeycomb-like cell around off-axis, and only about 5% of the POI distributed around middle axis, as shown in Figure 6. It should be noted that off-axis position was deviated from middle-axis about 1/4 of width of the structural cell. Therefore, mean values of DOP data in experiment were mainly dominated by the values obtained from the off-axis situation. Maybe the reason is that the simulation results obtained from off-axis situation are more close to the test results. The errors were mainly caused by the discrepancy between the projectiles with deformation and fracture in test and projectiles without any deformation in simulation. Figure 7 shows the histogram of DOP. As seen, the results basically demonstrated that the calibrated model leads to reasonable predictions. Dynamic response and damage mode of the HPS were observed during the overall penetration process in simulations. The DOP of middle caliber projectiles were 25~30% larger than that of small caliber projectiles.

3. Analysis and Discussion

3.1. Penetration Mode. The resistance of the HPS to penetration is related to its capacity to dissipate kinetic energy of projectile. During deep penetration, significant motion of the particles resulted in considerable compression and shear. Energy dissipation in shear was mainly due to friction and volume change as particles slide, roll, and climb over one

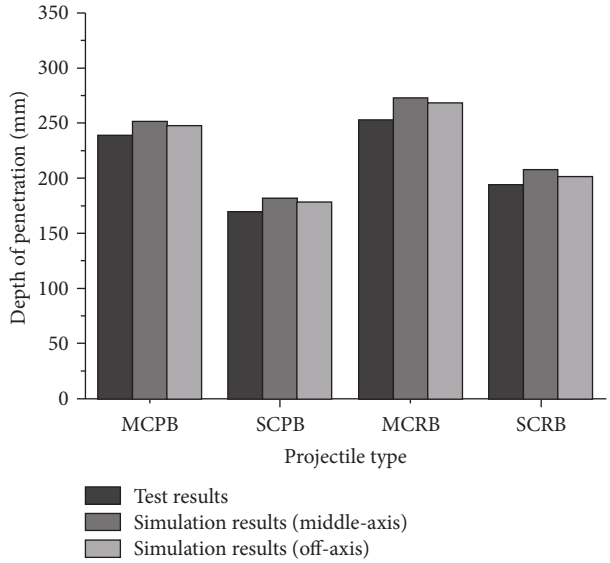

Figure 7: The contrast of DOP data.

another [17]. Friction between particles was elevated by the stress which exists in front of projectile nose. Volume change during shear led to pressure-volume work and energy dissipation. The subsequent creation of new surface area was an additional source of energy dissipation. These energy dissipation mechanisms form the basis for understanding projectile penetrating into sandy soil confined by HPS. Thus, the energy transfer during the penetration can be basically presented as below:

$$E_k = \frac{1}{2} m_p v^2 \Longrightarrow E_{\text{tear}} + E_{\text{fric}} + E_v + E_{\text{pm}} + E_{\text{therm}}, \tag{12}$$

where E_k denotes the kinetic energy of projectile, which is the function of mass m_p and the square of velocity v, and E_{tear} denotes the tearing energy of the strip, and E_v denotes the total energy dissipated by soil volume change, and E_{fric} denotes the frictional energy, and E_{pm} denotes the motion energy of sand particles, and E_{therm} denotes the thermal energy.

Besides, the mechanism may be approached from a phenomenological viewpoint for understanding the penetration process, as shown in Figure 8. The process can be divided into three stages: (1) contact and compression stage, (2) excavation stage, and (3) instability stage. The first stage refers to the perforation of strip and the generation of compression wave in sand particles. It had been found that a short projectile penetrating sand lost most of its energy as it sets sand particles in motion in initial stage of penetration [17]. During the second stage, particles were moving in two different forms: some of them were compressed on the windward side of projectile and some were released to the inner surface of front strip resulting in an upheaval around POI. Projectile instability occurred in the final stage, which was the deviation of the projectile from the axis of its trajectory [20], and the resisting forces introduced along the nose and length of the projectile will be nonsymmetric due to the influence of the heterogeneous nature of sandy soils. Actually, there are many factors inducing the deflection of projectile. The ballistic performance of Ti-6Al-4V-based homogeneous and "high-gradient" porous composite materials, obtained by hot isostatic pressing against long rod impact, was discussed in Nesterenko's monograph [21]. Powder-filled voids and rods induced a volume distributed, highly heterogeneous pattern of damage initiated by cavities and their interactions, replacing a few dominant shear bands that cause plugging in homogeneous material. As a result, deflection of the rod penetrator was induced. The resisting forces acted on the pressure center of the projectile. If the pressure center was located ahead of the center of mass, any deviation would produce a torque [22–24]. Once the projectile developed an angle within the sandy soil, the force was higher on the windward side, which could lead to a curved trajectory. In this stage, the cavity was formed at the leeward side of the projectile in sandy soil due to transient cavity effect, which is correlated with kinetic energy and instability of projectiles. The analysis of penetration process was validated by simulation results as shown in Figure 9.

3.2. The Effect of POI on Penetration. In simulations, POI was set to middle-axis position and off-axis position of the cell, respectively, to investigate the effect on the penetration. As shown in Figure 10, the strips of both sides of the cell were tighten up and separated from sandy soil when HPS was subjected to severe impact in such a short time. The tumbling of the projectiles can also be found in Figures 10, 11, 14, and 15 because of instability. The front strip and inner strip were both destroyed when the projectile penetrated from the position of off-axis as shown in Figures 11 and 15. The change of negative acceleration is shown in Figures 12 and 16.

By comparing Figure 10 with Figure 14, the cavity formed by MCPB was bigger than that formed by MCRB; the same phenomenon can also be found by comparing Figure 11 with

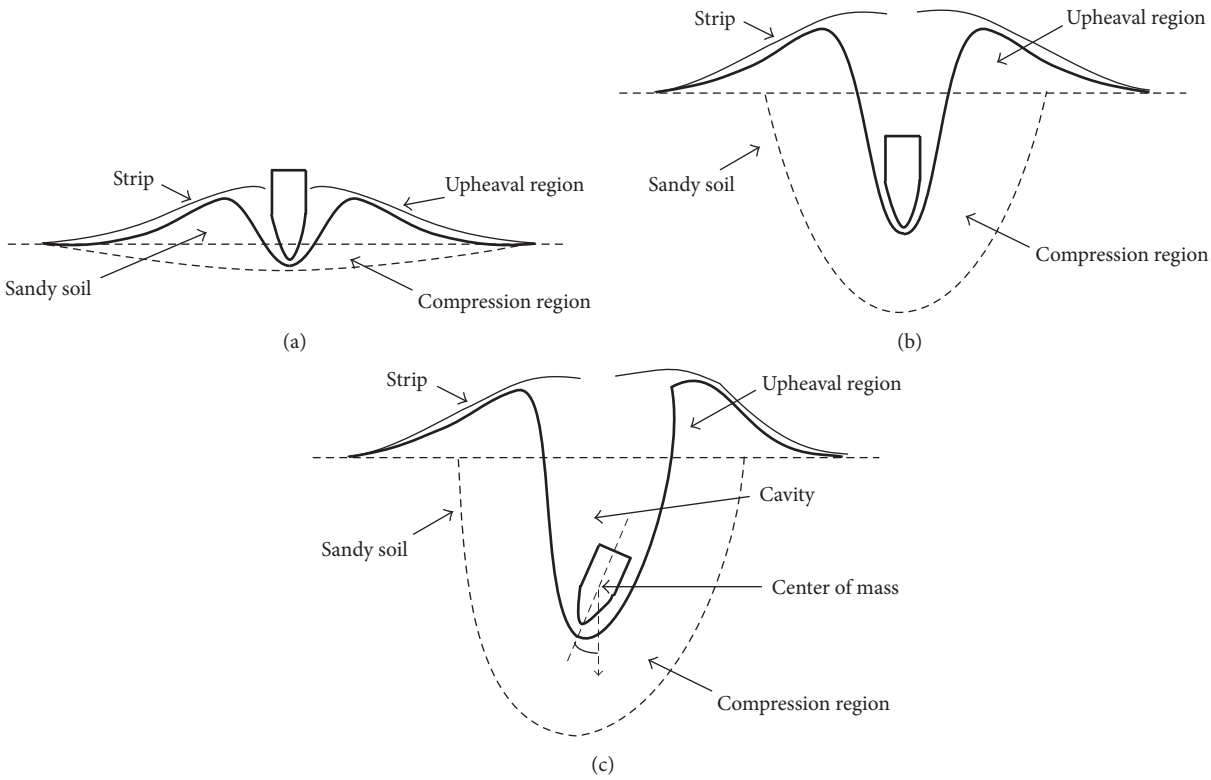

Figure 8: Penetration mode.

Figure 15. The bell-shape negative acceleration curves were formed as shown in Figure 16. It can be clearly found that the crest of off-axis curve was formed before that of middle-axis curve, which means that the instability occurred easily and early when the POI was set to off-axis position. Meanwhile, the DOP decreased compared with the case of middle-axis.

In Figures 13 and 17, it shows that the energy transfers in three parts including projectile, sandy soil, and strip, which were calculated automatically by the LS-PrePost. It shows that the kinetic energy of projectile dissipated into sandy soil largely and the strip slightly, and the former was greater than the sum of the latter for some energy went out as frictional energy and thermal energy. In the case of middle-axis, for MCPB, the transfer rates of kinetic energy of projectile dissipated in sandy soil and the strip were 72.32% and 3.92%, respectively. In the case of off-axis, the rates were 74.45% and 3.99%, respectively. For MCRB, the rates were 76.58% and 1.22%, respectively, in the case of middle-axis and 81.25% and 1.94%, respectively, in the case of off-axis. It is found that the rates in the case of off-axis were higher than that in the case of middle-axis. Thus, it can be inferred that approximate 45° angle of impact was formed in the case of off-axis, which has a certain influence on the ballistic stability, resulting in more kinetic energy of projectile dissipating in HPS and less depth of penetration. The total energy of sandy soil absorbed from projectile mainly transferred into motion energy of particles and the energy of soil volume change. It shows that the transfer rates of kinetic energy of MCPB dissipated in strip were higher than that of MCRB. But it is reversed for the transfer rates of kinetic energy dissipated in sandy soil. Besides, it seems that there is not much difference between two processes of energy dissipation in Figure 13. However, for MCRB, it is quite obvious that process of energy dissipation is different from each other, though the amount of energy that the projectile dissipated in sandy soil and strip is similar.

Meanwhile, under impact of MCRB, there is little change in strip around the POI due to the better penetration performance of ogive-nose rifle bullet, which was sharp enough to break through the strip and fast enough to make little influence on surrounding particles. However, the negative acceleration of MCRB is almost twice as much as that of MCPB due to the higher impulse and stronger inertia effect. Besides, the length-diameter ratio of MCRB is bigger than that of MCPB. Therefore, the resisting forces and the torque that act on MCRB would be greater than that acting on MCPB.

3.3. The Effect of Projectile Caliber on Penetration. The penetration process of SCPB seems relatively mild compared with that of SCRB as shown in Figures 18 and 19. The penetration process of SCRB seems the most severe one in all cases because its kinetic energy is tremendous compared with others. The strip was completely torn and rolled outward. Meanwhile, transient cavity formed by SCRB is bigger than that formed by others. Due to the higher muzzle velocity, SCRB have a great amount of kinetic energy. Hence, it suffered bigger negative acceleration which was twice or even four times as much as that of MCPB and MCRB during the penetration, as shown in Figure 20.

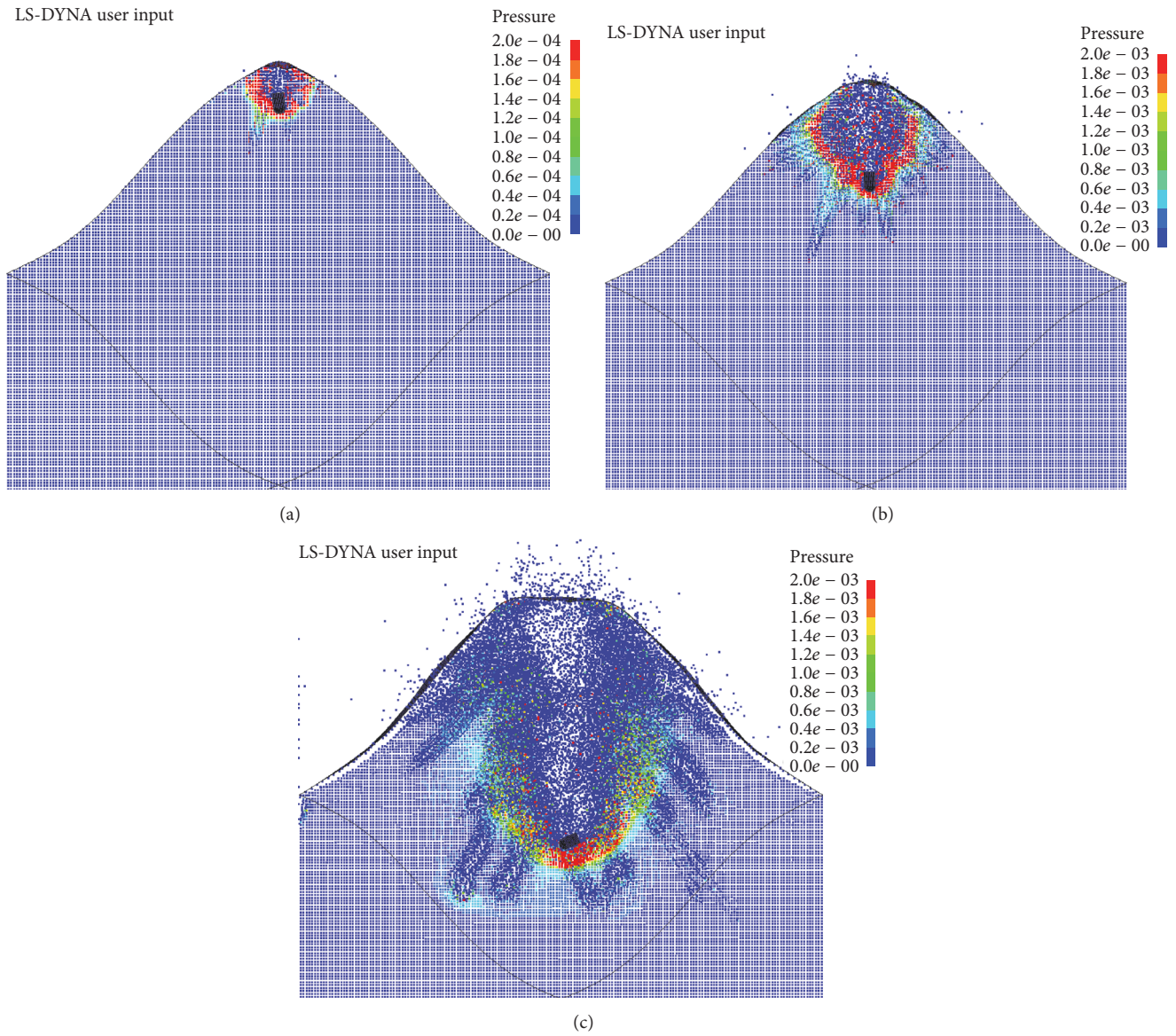

Figure 9: Pressure contour of penetration process.

In Figure 21, the amounts of energy dissipation differ sharply from each other because the initial kinetic energy of SCRB is much higher than that of SCPB. Both the processes of energy dissipation happened almost simultaneously. For SCPB, the transfer rates of kinetic energy of projectile dissipated in sandy soil and strip were 70.13% and 1.21%, respectively. For SCRB, the rates were 85.24% and 2.22%, respectively. It shows that the transfer rate of kinetic energy of SCRB dissipated in sandy soil is the highest in all cases.

3.4. The Effect of AOI on Penetration. AOI was defined as shown in Figure 6, which has certain randomness in most practical cases. In order to examine the effects of AOI on penetration, the simulations were carried out when the axis of projectile was normal to the strip in the case of off-axis.

As shown in Figures 22 and 23, it is easy to find that upheaval becomes more apparent, which was formed by sand particles released to the inner surface of front strip. The transient cavity formed by MCPB expanded periodically. The inner strip in both situations had not been damaged because the kinetic energy of projectile was completely dissipated before it reached the inner strip. The negative acceleration of projectile is shown in Figure 24. There were two crests formed in both curves, and the second crest of curve of MCRB was greater than that of curve of MCPB because of higher kinetic energy. In Figure 25, for MCPB, the transfer rates of kinetic energy of projectile dissipated in sandy soil and strip were 73.93% and 3.46%, respectively. For MCRB, the rates were 80.92% and 1.73%, respectively. The above rates of kinetic energy of projectile dissipated in sandy soil are between the

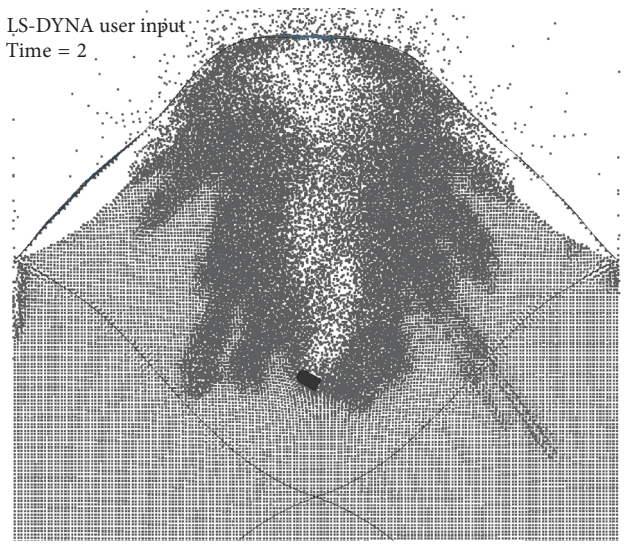

Figure 10: Penetration from middle-axis by MCPB.

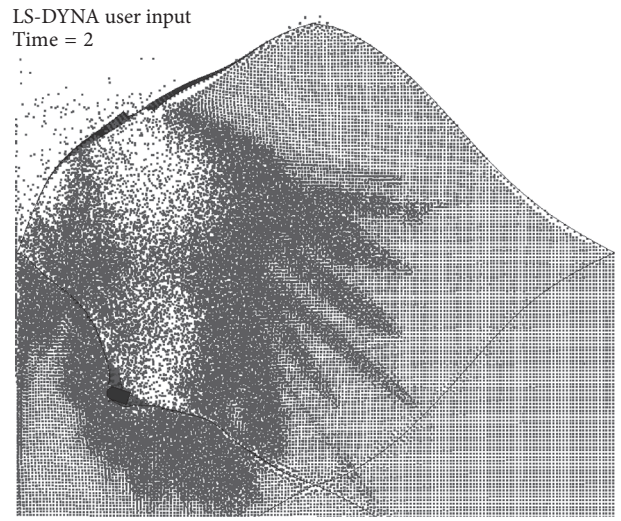

Figure 11: Penetration from off-axis by MCPB.

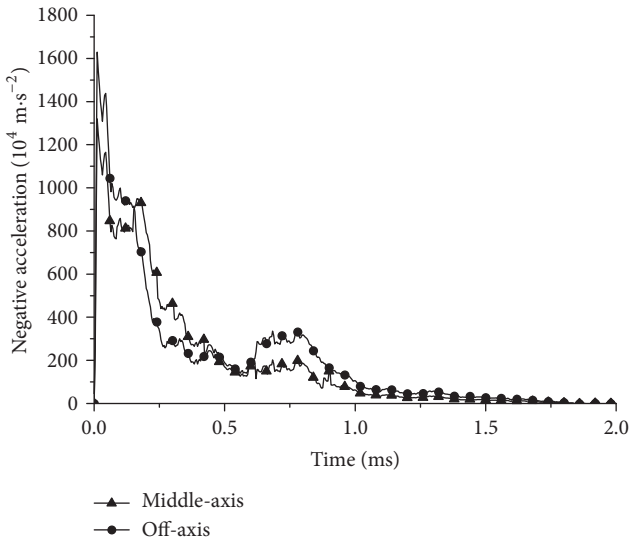

Figure 12: Negative acceleration of MCPB from different POI.

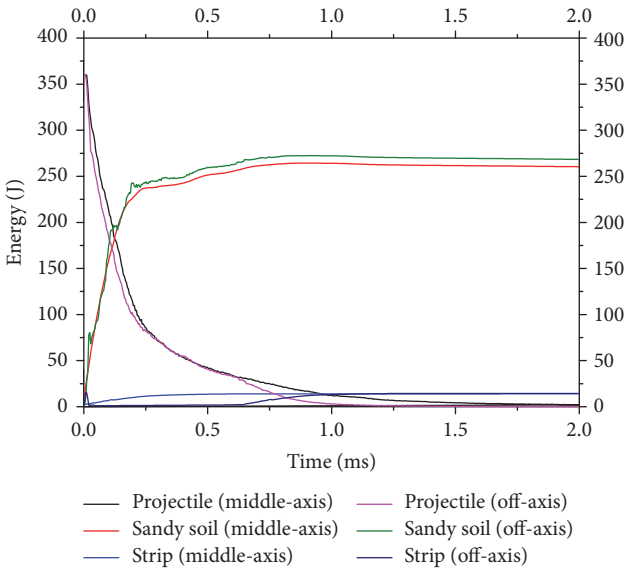

Figure 13: Energy transfer during the penetration.

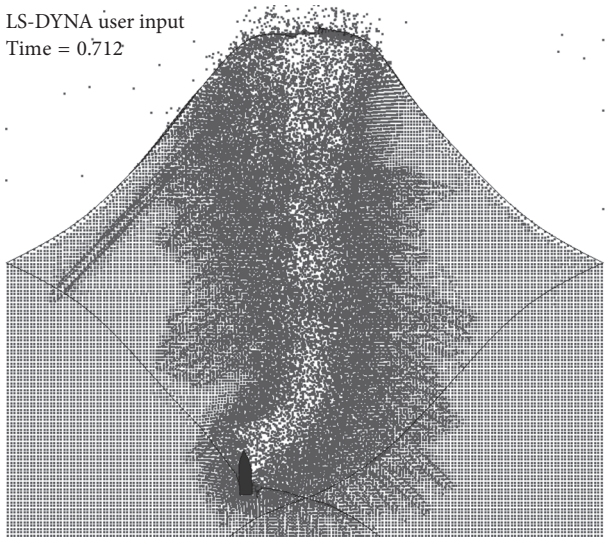

Figure 14: Penetration from middle-axis by MCRB.

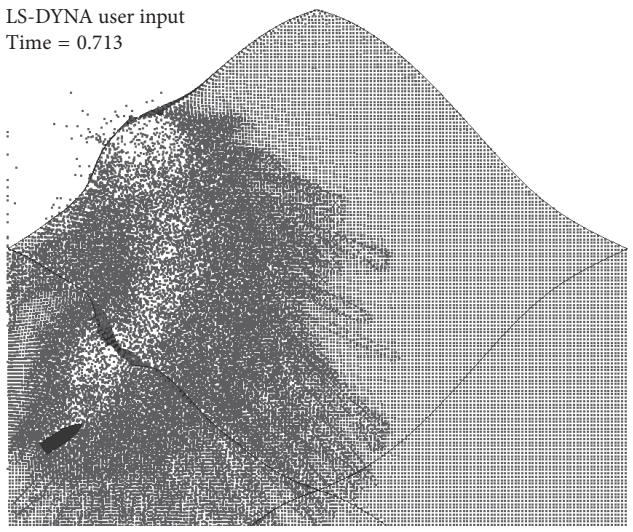

Figure 15: Penetration from off-axis by MCRB.

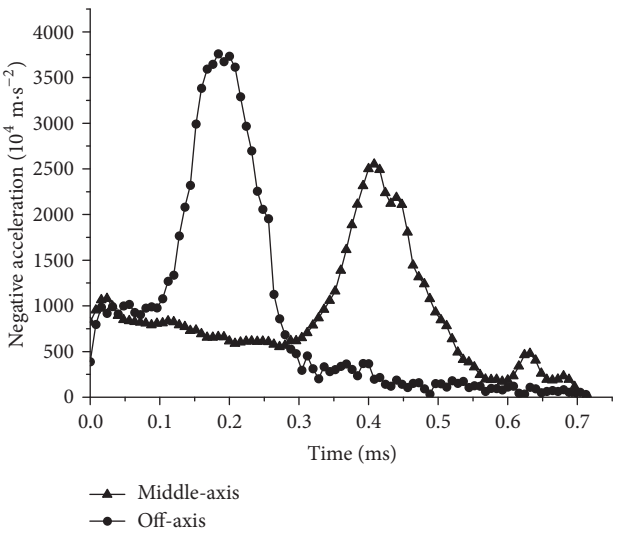

Figure 16: Negative acceleration of MCRB from different POI.

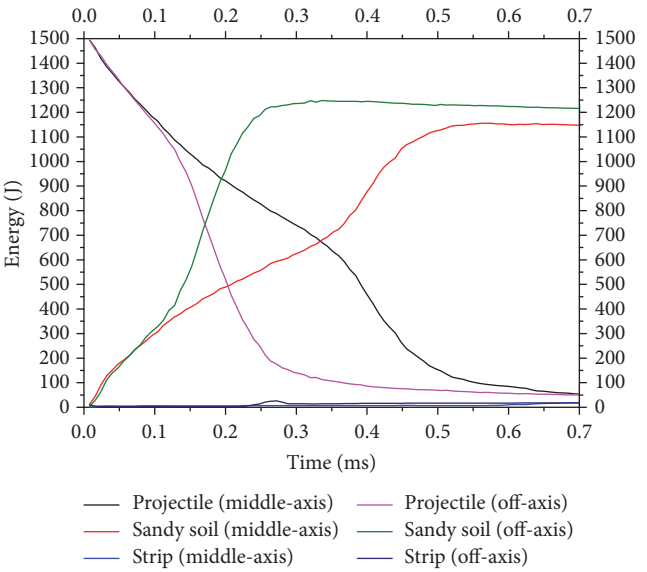

Figure 17: Energy transfer during the penetration.

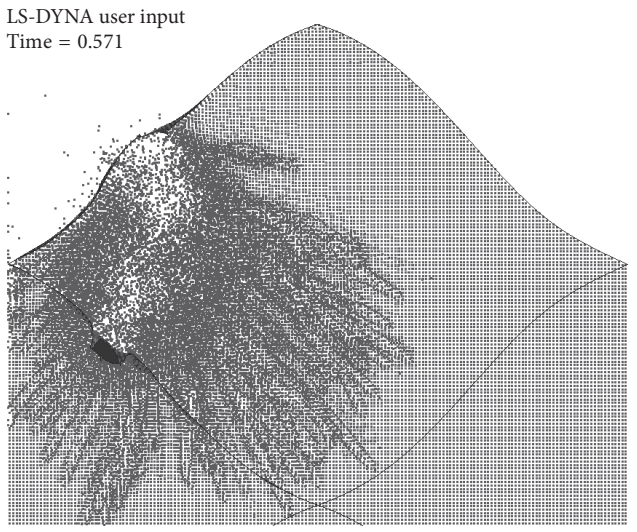

Figure 18: Penetration from off-axis by SCPB.

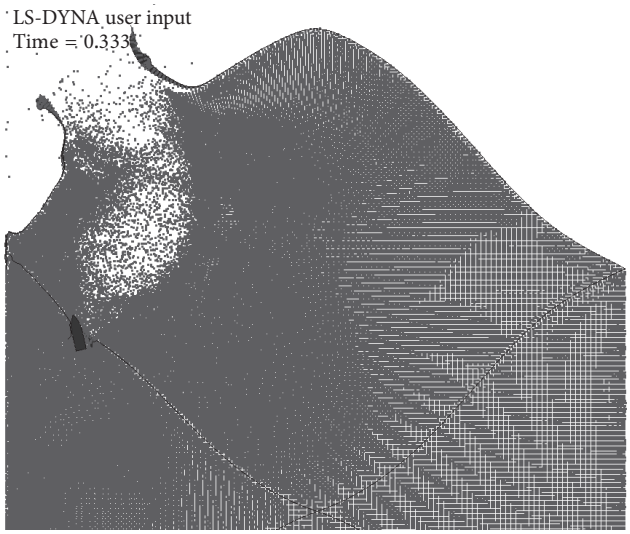

Figure 19: Penetration from off-axis by SCRB.

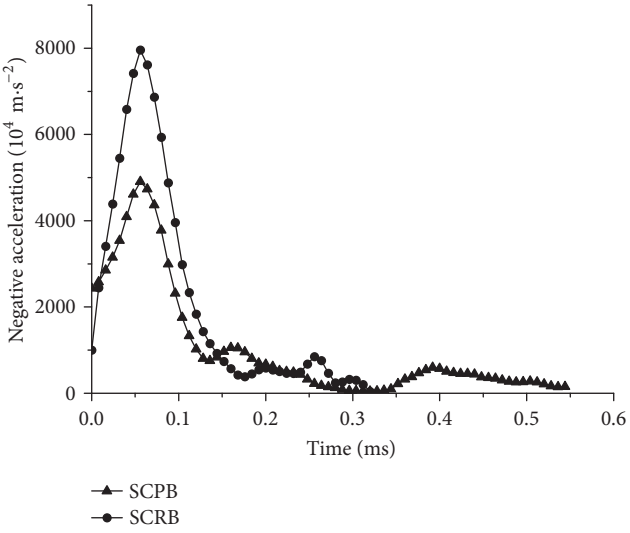

Figure 20: Negative acceleration of SCPB and SCRB.

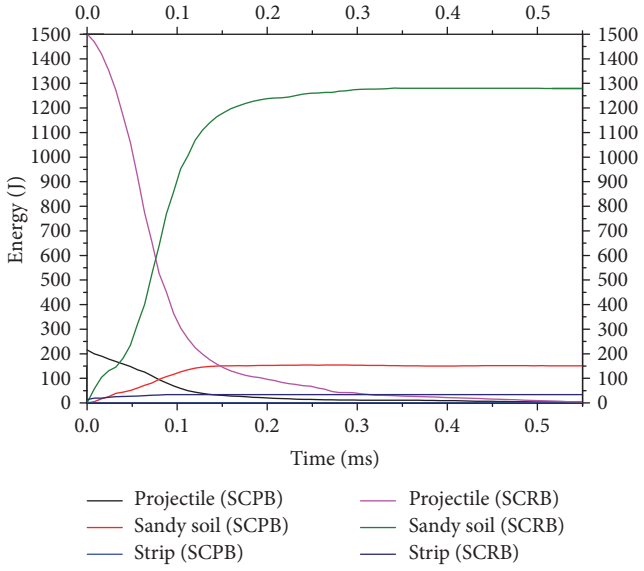

Figure 21: Energy transfer during the penetration.

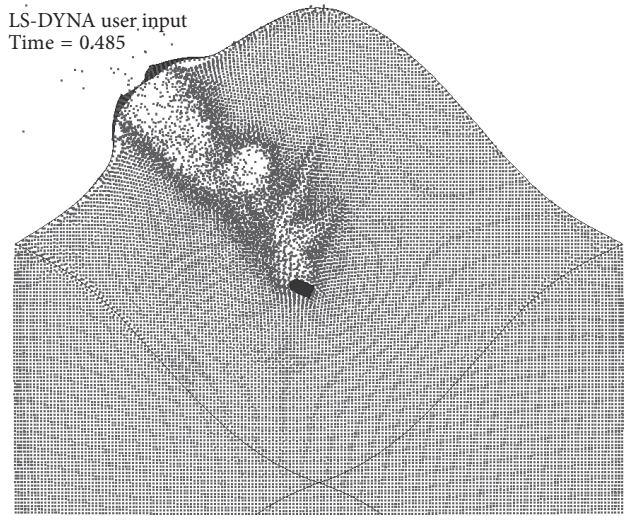

Figure 22: Penetration by MCPB when axis of projectile was normal to the strip.

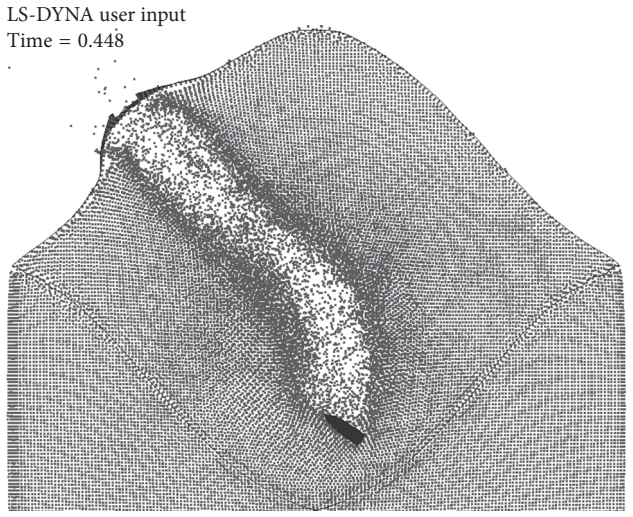

Figure 23: Penetration by MCRB when axis of projectile was normal to the strip.

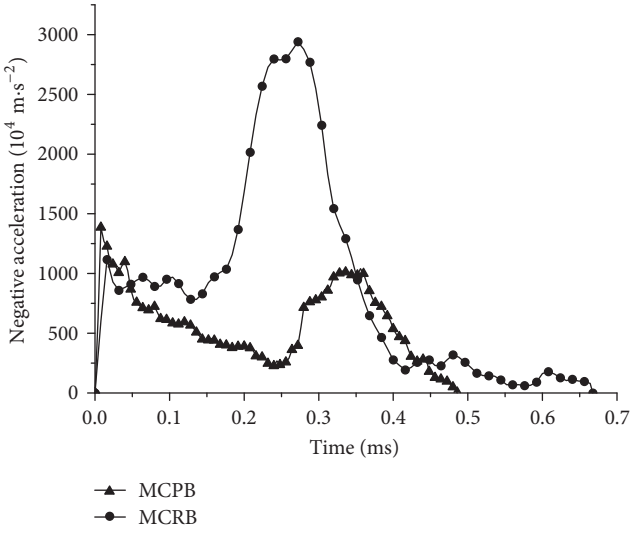

Figure 24: Negative acceleration of MCPB and MCRB.

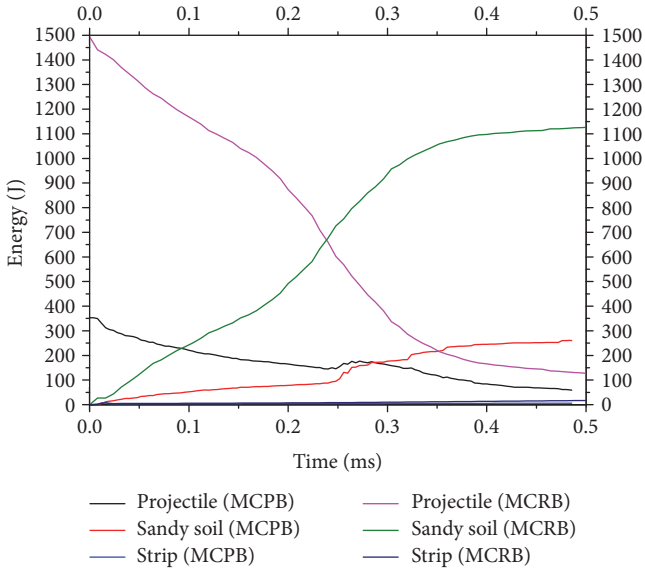

Figure 25: Energy transfer during the penetration.

rates mentioned in Section 3.1, which are the cases of middle-axis and off-axis, respectively.

4. Conclusions

For further research on the penetration resistance of the HPS (Honeycomb-like Protective Structure), more cases were simulated considering the key factors influencing the penetration including point of impact, angle of impact, and projectile caliber. Simulation results show that (a) the resisting forces and the torque that act on the long rod projectile would be greater than those acting on the short one when instability occurred, (b) approximate 45° angle of impact was formed in the case of off-axis, which has a certain influence on the ballistic stability, resulting in more kinetic energy of projectile dissipating in HPS and less depth of penetration, and (c) the kinetic energy of projectile energy dissipated in sandy soil largely and strip slightly, and the former was greater than the sum of the latter. For refining the model and improving accuracy of simulation, the results need more experimental validation in future research.

Conflicts of Interest

The authors declare that they have no conflicts of interest.

Acknowledgments

This work was supported by the National Natural Science Foundation of China (Grants nos. 51378495 and 51408602).

References

[1] S. Lambert, F. Stéphane, F. Nicot, and P. Gotteland, "Uniaxial compressive behavior of scrapped tire and sand-filled wire netted geocell with a geotextile envelope," *Geotextiles and Geomembranes*, vol. 29, no. 5, pp. 483–490, 2011.

[2] T. Børvik, A. G. Hanssen, S. Dey, H. Langberg, and M. Langseth, "On the ballistic and blast load response of a 20 ft ISO container protected with aluminium panels filled with a local mass—phase I: design of protective system," *Engineering Structures*, vol. 30, no. 6, pp. 1605–1620, 2008.

[3] T. Børvik, A. Burbach, H. Langberg, and M. Langseth, "On the ballistic and blast load response of a 20ft ISO container protected with aluminium panels filled with a local mass—phase II: validation of protective system," *Engineering Structures*, vol. 30, no. 6, pp. 1621–1631, 2008.

[4] K. Scherbatiuk and N. Rattanawangcharoen, "Experimental testing and numerical modeling of soil-filled concertainer walls," *Engineering Structures*, vol. 30, no. 12, pp. 3545–3554, 2008.

[5] A. Van Vooren, J. Borg, H. Sandusky, and J. Felts, "Sand penetration: A near nose investigation of a sand penetration event," in *Proceedings of the 12th Hypervelocity Impact Symposium, HVIS 2012*, pp. 601–607, usa, September 2012.

[6] T. Abe, S. Sato, and K. Funabiki, "Experimental study on performance of vehicle penetrating into sand-like soil," in *Proceedings of the 43rd Fluid Dynamics Conference*, San Diego, Calif, USA, 2013.

[7] G. Ben-Dor, A. Dubinsky, and T. Elperin, "Engineering models of high speed penetration into geological shields," *Central European Journal of Engineering*, vol. 4, no. 1, pp. 1–19, 2014.

[8] J. K. Holmen, T. Børvik, and O. S. Hopperstad, "Experiments and simulations of empty and sand-filled aluminum alloy panels subjected to ballistic impact," *Engineering Structures*, vol. 130, pp. 216–228, 2017.

[9] T. Børvik, S. Dey, and L. Olovsson, "Penetration of granular materials by small-arms bullets," *International Journal of Impact Engineering*, vol. 75, pp. 123–139, 2015.

[10] C. Zhao and M. Zang, "Application of the FEM/DEM and alternately moving road method to the simulation of tire-sand interactions," *Journal of Terramechanics*, vol. 72, pp. 27–38, 2017.

[11] S. Swaddiwudhipong, M. J. Islam, and Z. S. Liu, "High velocity penetration/perforation using coupled smooth particle hydrodynamics-finite element method," *International Journal of Protective Structures*, vol. 1, no. 4, pp. 489–506, 2010.

[12] S. Koneshwaran, D. P. Thambiratnam, and C. Gallage, "Blast Response of Segmented Bored Tunnel using Coupled SPH-FE Method," *Structures*, vol. 2, pp. 58–71, 2015.

[13] K. Krishnan, S. Sockalingam, S. Bansal, and S. D. Rajan, "Numerical simulation of ceramic composite armor subjected to ballistic impact," *Composites Part B: Engineering*, vol. 41, no. 8, pp. 583–593, 2010.

[14] B. S. Thatte, G. S. Chandekar, A. D. Kelkar, and P. Chaphalkar, "Studies on behavior of carbon and fiberglass epoxy composite laminates under low velocity impact loading using LS-DYNA," in *in Proceeding of 10th International LS-DYNA Users Conference*, Dearborn, Mich, USA, 2008.

[15] *LS-DYNA Keyword Users Manual (Version 971 R6.1.0)*, Livermore Software Technology Corporation, Livermore, Calif, USA, 2012.

[16] *LS-DYNA Theoretical Manual*, Livermore Software Technology Corporation, Livermore, Cali, USA, 1998.

[17] M. Omidvar, M. Iskander, and S. Bless, "Response of granular media to rapid penetration," *International Journal of Impact Engineering*, vol. 66, pp. 60–82, 2014.

[18] M. Omidvar, M. Iskander, and S. Bless, "Stress-strain behavior of sand at high strain rates," *International Journal of Impact Engineering*, vol. 49, pp. 192–213, 2012.

[19] K. Wada, H. Senshu, and T. Matsui, "Numerical simulation of impact cratering on granular material," *Chemie Ingenieur Technik*, vol. 42, no. 2, pp. 528–545, 2005.

[20] Q. M. Li and E. A. Flores-Johnson, "Hard projectile penetration and trajectory stability," *International Journal of Impact Engineering*, vol. 38, no. 10, pp. 815–823, 2011.

[21] V. F. Nesterenko, *Dynamics of Heterogeneous Materials*, Springer, New York, NY, USA, 2001.

[22] J. P. Borg, M. P. Morrissey, C. A. Perich, T. J. Vogler, and L. C. Chhabildas, "In situ velocity and stress characterization of a projectile penetrating a sand target: Experimental measurements and continuum simulations," *International Journal of Impact Engineering*, vol. 51, pp. 23–35, 2013.

[23] S. K. Dwivedi, R. D. Teeter, C. W. Felice, and Y. M. Gupta, "Two dimensional mesoscale simulations of projectile instability during penetration in dry sand," *Journal of Applied Physics*, vol. 104, no. 8, Article ID 083502, 2008.

[24] A. L. Collins, J. W. Addiss, S. M. Walley et al., "The effect of rod nose shape on the internal flow fields during the ballistic penetration of sand," *International Journal of Impact Engineering*, vol. 38, no. 12, pp. 951–963, 2011.